

## DEVELOPMENT OF AN INDUSTRIAL ROBOTIC ARM EDUCATION KIT BASED ON OBJECT RECOGNITION AND ROBOT KINEMATICS FOR ENGINEERS

Mustafa Yusuf YILDIRIM<sup>1, +</sup>, Mustafa ANUTGAN<sup>2</sup>

<sup>1</sup>Erciyes University, Engineering Faculty, Mechatronics Engineering Department,  
Kayseri Türkiye

<sup>2</sup>Karabuk University, Technology Faculty, Mechatronics Engineering Department,  
Karabuk Türkiye

myyildirim@erciyes.edu.tr, mustafaanutgan@karabuk.edu.tr

### Abstract

Robotic vision makes systems in the industry more advantageous regarding practicality and flexibility. For this reason, it is essential to provide the necessary training for the standard use of vision based robotic systems on production lines. In this article, it is aimed to design a low cost computer vision based industrial robotic arm education kit with eye-to-hand configuration. This kit is based on classifying and stacking products in random locations in a short time, making them ready for industrial operations or logistics. In the development phase of the system, firstly, motion simulation of the robotic arm was performed and then, experimental setup was established, and the performance of the system was tested by experimental studies. This system, which operates with a great success rate, has been made available for use within the scope of education. Regarding the use of the system for educational purposes, this kit supports theoretical lessons by reviewing object recognition (vision systems), forward - inverse kinematics, and trajectory planning (robot kinematics) and running the system several times. Thus, engineering students are expected to approach the industry more consciously and to develop the industry. It can also be used for training of relevant engineers in the institution where vision based robotic systems are available.

**Keywords:** Education Kit, Stereo Vision, Robotic Arm, Object Recognition and Classification, Pick-and-Place Task

+ This paper has been presented at the ICAT'20 (9th International Conference on Advanced Technologies) held in Istanbul (Turkey), August 10-12, 2020.

## **1. Introduction**

Applications in engineering education is an important issue for the industry. Many kits have been developed for these applications today. Students become familiar with the industry with these kits. Robotic arms are also a part of the industry and can be used in many areas. One of the areas where robotic arms are mostly used in industry is the pick-and-place task. In robotic-system-based automated production lines for pick-and-place tasks, a robotic arm holds the products whose positions are detected by the sensors and then transports them to another place. However, the accuracy and performance of this task depend on the programmer or operator. Moreover, different systems or programs are required for each different situation. For example; a robotic arm behaves very efficiently when the products come in the desired directions and angles, while it cannot accurately pick-and-place the products coming with different from desired directions or angles. In order to solve this problem, recently, studies have started for controlling robotic arms used in pick-and-place tasks by means of computer vision algorithms. The use of these provides more accurate and faster real-time process control. In this way, even in case of a situation other than that is expected by the system pick-and-place tasks can be performed correctly (flexibility problem). Instead of sensor - based feedback, the use of this vision-based feedback eliminates the flexibility problem in repetitive pick-and-place tasks. These systems provide an advantage over production speed, hardware complexity and human errors. Moreover, this is becoming extremely important for the industrial 4.0 revolution and dark factories [1]. The reason to prefer pick-and-place task for the robotic arm in this kit is that according to Technavio reports, pick-and-place tasks take the first place in the application distribution of collaborative robotic systems in 2016 with a rate of 32% [2]. Furthermore, according to the same reports, visual systems are again in the first place in the usage distribution of sensor types in industrial robotic systems in 2016 with a rate of 62%. The use of these visual systems is expected to increase by 8.9% until 2021 [3].

Some stereo vision based industrial robotic system studies in the literature can be explained as follows: Şenel et al. separated the faulty products passing over a production line with the help of an embedded system software and a robotic arm [4]. Lin et al. developed an object handling algorithm for different geometric-shaped objects using a stereo camera system and an industrial robot [5]. Taryudi et al. calibrated the

camera and robotic arm coordinate transformation using an adaptive network-based fuzzy inference system (ANFIS) method [6]. Shi et al. offered a hybrid vision-based robotic system in which both eye-to-hand and eye-in-hand systems are used together to perform the correct positioning of the products moving on the production line [7]. Chang et al. developed a vision-based robotic system for contour tracking of an object with unknown geometrical shape [8]. Ali et al. aimed to combine the visual systems with a robotic arm named Scorbot - ER 9 Pro, and for this purpose, they mounted a camera on end effector of the robotic arm [9]. Luo et al. added the computer vision system to perform the hold-and-place task on the industrial robot arms. Eye to hand configuration has been adopted in this system [10]. Fei et al. developed a 3D object scanning system to identify complex shaped objects. In this system, eye in hand configuration has been adopted [11]. Kang et al. developed a vision-based robotic system for bin picking. They used dual arm for this. They preferred a stereo vision system for detection of objects [12]. Dinham et al. developed a method for welding robots that includes simultaneous calibration of robot and camera systems. The authors concluded that this developed system increased sensitivity in robotic systems that arc welding [13].

These studies in the literature have contributed by combining robotic systems with cameras. However, there is a lack of studies on computer vision based robotic systems that are suitable for mass production and prepared for educational purposes in the literature. In order to develop automatic dark factories, vision based robotic systems should be used more widely in the industry. Thus, it is of great importance to provide the necessary trainings in the related institutions for the standard use of vision based robotic systems in production lines. This paper aims to develop low cost industrial robotic arm education kit with eye-to-hand configuration for vision based robotic systems. The system can be used within the scope of education in the fields of engineering. Thus, theoretical lessons of object recognition, forward - inverse kinematics, and trajectory planning can be supported by using this kit for engineering students. It can also be used for training of engineers in the institution where vision based robotic systems are available or newly installed. As a result, computer vision based robotic systems can be integrated into industries more easily and quickly; access to automatic dark factories can be provided faster. In addition, the system developed in

this paper may be the beginning of collaborative robotic systems for use in industry.

It is possible to list the sections of the study as follows: In the second section, material and method is presented. The third section shows the experimental studies and results. The fourth section is conclusion.

## **2. Materials and Method**

### *2.1 Materials*

The developed kit is run with MATLAB editor. The system performs the classification of the objects according to their colors. Figure 1 shows the experimental setup and objects used in this paper. Tinkercat Braccio Robot has been preferred as the robotic arm since it is low-cost, efficient at pick-and-place tasks and suitable for size of the experimental setup. This robotic arm uses four RC servo motors, three of which are joint motors of base, shoulder and elbow. The other motor is the end effector motor which enables the end effector to be switched on and off. Since end effector does not add any degree of freedom to the robotic arm and the joint connecting end effector to body is not used in this paper, the preferred robotic arm is defined as having three degrees of freedom. Two separate Logitech C310 webcams have been preferred as the stereo camera system since they are small-sized, supported by MATLAB and low-cost in comparison to stereo cameras. These cameras have been mounted as adjacent each other to the upper part of the experimental setup by tight-fitting, thus a stereo camera system has been created. The coordinate center of the stereo camera system is the lens center of the left camera according to the view direction. Two Arduino boards (Uno and Mega 2560) have been preferred as control unit since they are low-cost and suitable in respect to both MATLAB and motor driver boards. Adafruit motor drive modules have been preferred as the motor driver boards since these modules are supported by MATLAB. Each module can control two motors and four motors of the robotic arm are used in this kit. For this reason, the system has two Arduino boards. The system is only controlled by MATLAB editor performing Arduino-MATLAB configuration independently of Arduino IDE. Two 5V-4A DC adapters are used as the power supplies since the motors of the robotic arm run with 5V-4A. Three 20k potentiometers are used for real-time joint position measurements.

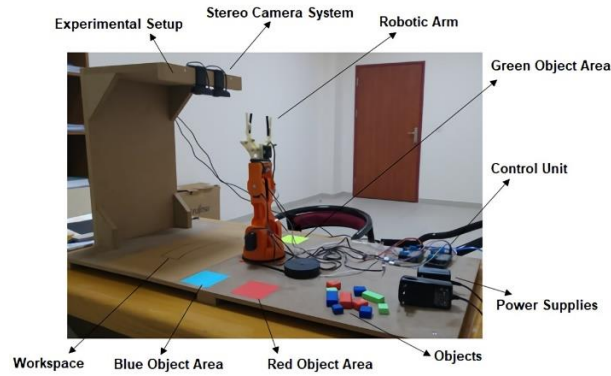


Figure 1. Experimental setup and objects

## 2.2 Preparatory Studies

### 2.2.1. Motion Simulation of the Robotic Arm

The movement of the robotic arm was simulated to reach a certain point. For this purpose, CAD model of the robotic arm was created as shown in Figure 2.

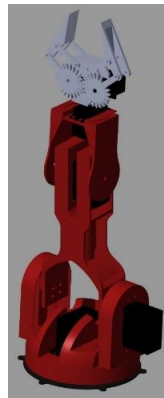


Figure 2. CAD model of the robotic arm

This model was transferred to MATLAB Simulink as a mechanical model. This Simulink model contains set values and PID controllers for each joint, robotic arm subsystem, scaling blocks, and monitor showing system responses. In the robotic arm subsystem, there is the joint based mechanical model of the robotic arm. In the mechanical model, motion is provided by PWM input and sensed position for each joint. Figure 3 shows the Simulink model, Figure 4 shows the robotic arm subsystem.

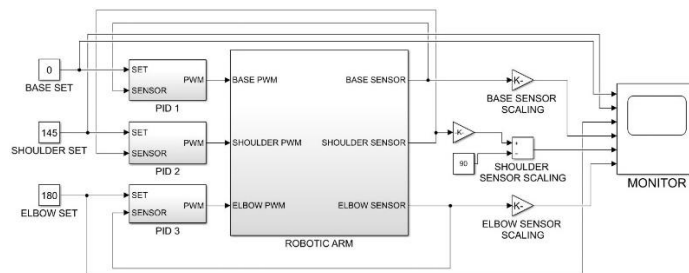


Figure 3. The Simulink model

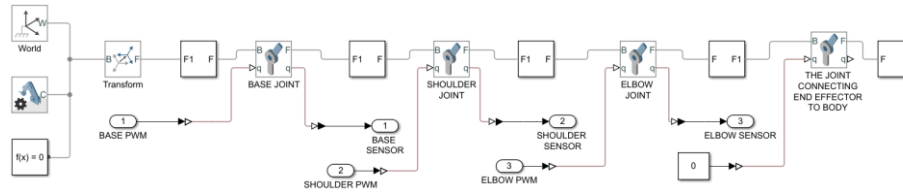


Figure 4. Robotic arm subsystem

Developed Simulink model was created to bring the base angle of the robotic arm to 0 degree, the shoulder angle to 145 degrees, and the elbow angle to 180 degrees. PID controller was designed for each joint. In PID controllers, the proportional coefficient was set to 0.33, the integral coefficient to 273 and the derivative coefficient to 0. As a result, each joint successfully reached the desired angle values without overshoot. Figure 5 shows the position based system responses of the PID controlled joints [14].

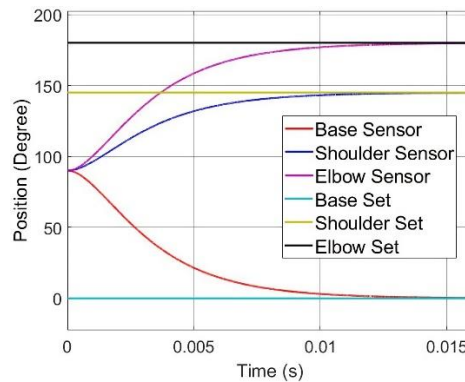


Figure 5. CAD model of the robotic arm

### 2.2.2. Calibration of the Stereo Camera System

Calibration of the stereo camera system is necessary to determine 3D position of objects. 12 photos were obtained from the cameras using a checkerboard. The calibration was performed using these photos and MATLAB Stereo Camera Calibrator Toolbox. Thus, results of the calibration (internal and external parameters of camera system) have been obtained. Figure 6 shows the coordinate system of the cameras [15]-[16].

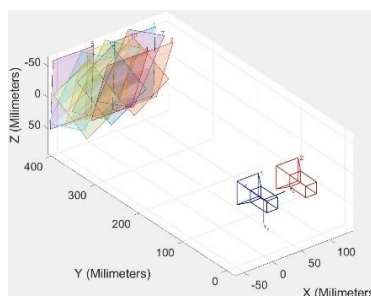


Figure 6. Coordinate system of the cameras

### 2.2.3. Workspace of the Robotic Arm

Workspace of the robotic arm was obtained, and the common area on the floor of the experimental setup was determined. Figure 7 shows the workspace of the robotic arm on the experimental setup, and Figure 8 shows the common area of the robotic arm and the stereo camera system onto the base of the experimental setup.

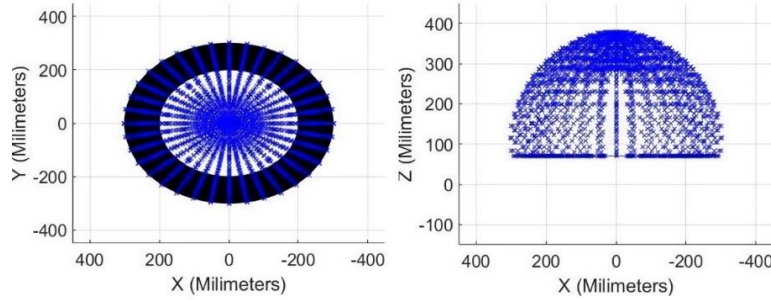


Figure 7. The workspace of the robotic arm on the experimental setup

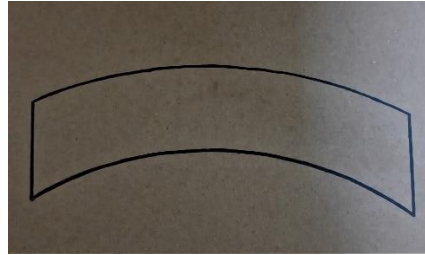


Figure 8. Common area of the robotic arm and the stereo camera system onto the base of the experimental setup

### 2.2.4. Real-Time Joint Position Measurement

Being sure about how much the joint motors actually rotate is an important issue. In this kit, joint positions are measured with the help of potentiometers. Potentiometers make instant measurements during the movement of the robotic arm. The potentiometers in the shoulder and elbow joints have been mounted on the joint axes. However, since the base joint is not suitable, the measurement is made by attaching the potentiometer to a belt-pulley system. The diameter of the pulley is 85 mm. Reduction ratio is 1.294 which seems to be quite successful for the position measurement with a potentiometer. Interpolation method is used for measurements. Equations 1, 2 and 3 measures joint positions depending on voltages.

$$\theta_{\text{base(measurement)}} = \frac{180.(4.999 - V_{\text{base}})}{4.6431} \quad (1)$$

$$\theta_{\text{shoulder(measurement)}} = \frac{140.V_{\text{shoulder}} - 45.088}{2.6435} \quad (2)$$

$$\theta_{\text{elbow(measurement)}} = \frac{180.(V_{\text{elbow}} - 0.7134)}{3.7331} \quad (3)$$

These equations were checked by a test where the trajectory was planned with a fifth order polynomial from the minimum angle value of the joints to the maximum angle value. Then, the motors were operated according to these trajectories. Measurements were also performed at the same time. The joints followed the trajectories successfully. The margins of error are due to some mechanical losses. Figures 9 (a), (b) and (c) show test results of real-time joint position measurements of base joint, shoulder joint and elbow joint.

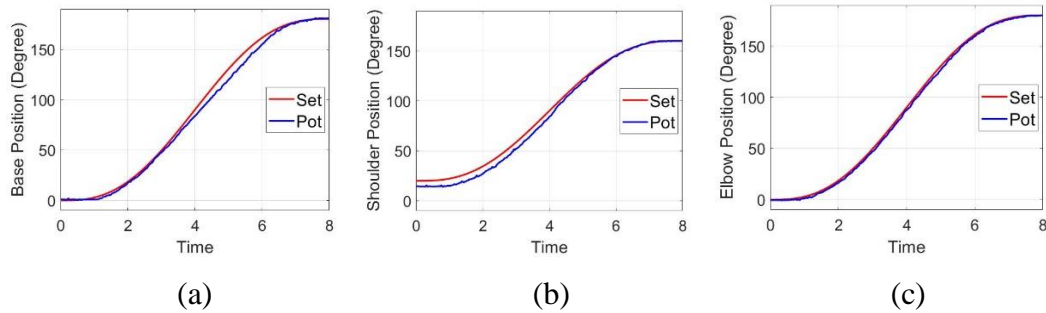


Figure 9. Test results of real-time joint position measurements of (a) base joint, (b) shoulder joint and (c) elbow joint

### 2.3 Method

#### 2.3.1. Recognition of Color and Position of Objects

RGB color space is used in this kit to detect the colors of the objects. Detection of the blue color is performed by subtracting the blue color from the image. The same method applies to green and red colors. The pixel coordinates of the objects are obtained by placing a plus sign in the center of the objects. The number of objects is also calculated. Triangulation method, which is important for depth information, is used in this kit to determine 3D coordinates of the objects by using the pixel coordinates on both camera images. The triangulation method requires results of the calibration and pixel coordinates of the objects. Figure 10 shows color detection with the stereo camera system.

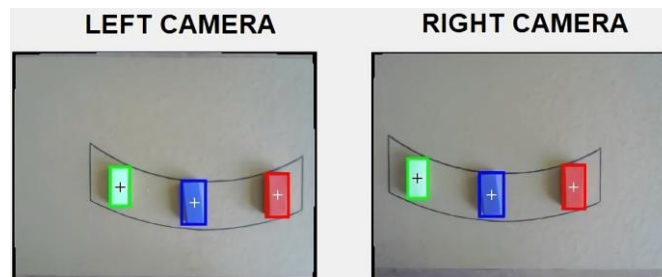




Figure 10. Color detection with the stereo camera system

### 2.3.2. Coordinate Transformation between Stereo Camera System and Robotic Arm

Since coordinate centers of the robotic arm and the stereo camera system are in different directions and positions, position of the objects relative to the robotic arm must be calculated. The positions obtained by the stereo camera system is converted to corresponding positions in the robotic arm coordinate system with the help of coordinate transformation. Figure 11 shows the coordinate systems of the stereo camera system and the robotic arm. In equation 4, the coordinate transformation of the system is given [17].

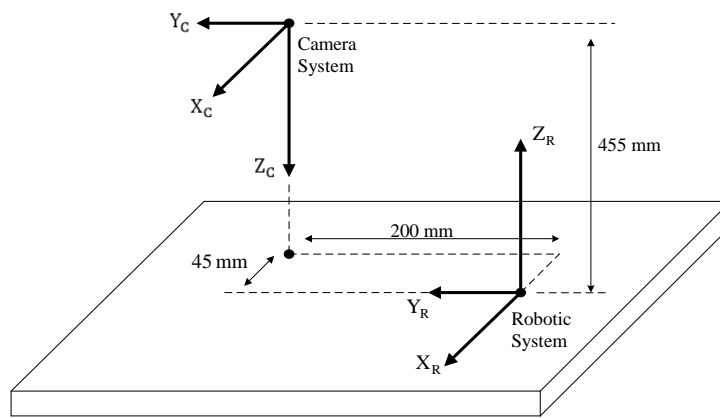


Figure 11. The coordinate systems of the stereo camera system and the robotic arm

$$\begin{bmatrix} x_R \\ y_R \\ z_R \end{bmatrix} = \begin{bmatrix} x_C - 45 \\ y_C + 200 \\ 455 - z_C \end{bmatrix} \quad (4)$$

Where:  $x_R, y_R, z_R$  are the positions of an object relative to the robotic arm on the x, y and z axes. Likewise,  $x_C, y_C, z_C$  are the positions of the object relative to the stereo camera system on the x, y and z axes.

### 2.3.3. Inverse Kinematics of the Robotic Arm

In this kit, joint angles have been calculated by inverse kinematics using positions of the objects relative to the robotic arm. Figure 12 shows a representative drawing of the robotic arm and joint frames.

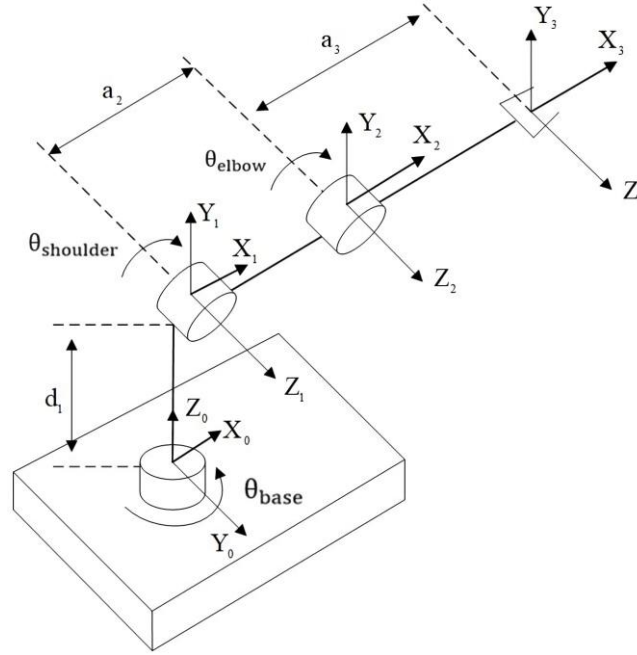


Figure 12. Representative drawing of the robotic arm and joint frames. The x-y-z axes represent joint frames;  $\theta_{base}$ ,  $\theta_{shoulder}$ ,  $\theta_{elbow}$  represent rotation angles of these joints;  $d_1$ ,  $a_2$ ,  $a_3$  represent the Denavit-Hartenberg (DH) parameters. DH parameters of the robotic arm created by using joint frames are shown in Table 1 [17]

Table 1. DH parameters of the robotic arm

<b>i</b>	<b><math>\alpha_{i-1}</math></b>	<b><math>a_{i-1}</math></b>	<b><math>d_i</math></b>	<b><math>\theta_i</math></b>	<b>Variable</b>
<b>1</b>	90	0	$d_1$	$\theta_{base}$	$\theta_{base}$
<b>2</b>	0	$a_2$	0	$\theta_{shoulder}$	$\theta_{shoulder}$
<b>3</b>	0	$a_3$	0	$\theta_{elbow}$	$\theta_{elbow}$

The values of the DH parameters are shown in Equations 5, 6 and 7.

$$d_1 = 70 \text{ mm} \quad (5)$$

$$a_2 = 130 \text{ mm} \quad (6)$$

$$a_3 = 180 \text{ mm} \quad (7)$$

The general transformation matrix in Equation 8 was used for the transformation matrix of each joint [18]. As a result of inverse kinematic calculations, 8 sets of solution were obtained. These solutions were simulated by 30 experiments with forward kinematics to verify and only one of the solutions is the correct position in each experiment. Using this solution, general expressions of the joints angles were obtained. The system directly uses these general expressions shown in Equations 9, 10 and 11.

$${}^{i-1}T = \begin{bmatrix} \cos(\theta_i) & -\cos(\alpha_{i-1}) \cdot \sin(\theta_i) & \sin(\alpha_{i-1}) \cdot \sin(\theta_i) & a_{i-1} \cdot \cos(\theta_i) \\ \sin(\theta_i) & \cos(\alpha_{i-1}) \cdot \cos(\theta_i) & -\sin(\alpha_{i-1}) \cdot \cos(\theta_i) & a_{i-1} \cdot \sin(\theta_i) \\ 0 & \sin(\alpha_{i-1}) & \cos(\alpha_{i-1}) & d_i \\ 0 & 0 & 0 & 1 \end{bmatrix} \quad (8)$$

$$\theta_{\text{base}} = \text{Atan2}(p_y, p_x) \quad (9)$$

$$\theta_{\text{elbow}} = \text{Atan2}(-\sqrt{1-f^2}, f) \quad (10)$$

$$\theta_{\text{shoulder}} = \text{Atan2}(a_2 + f \cdot a_3, a_3 \cdot \sin(\theta_{\text{elbow}})) \\ + \text{Atan2}\left(-\sqrt{(a_2 + f \cdot a_3)^2 + (a_3 \cdot \sin(\theta_{\text{elbow}}))^2} - h^2, h\right) \quad (11)$$

The intermediate expressions  $f$  and  $h$  are shown in Equations 12 and 13.

$$f = \frac{(p_x \cos(\theta_{\text{base}}) + p_y \sin(\theta_{\text{base}}))^2 + h^2 - a_2^2 - a_3^2}{2a_2 a_3} \quad (12)$$

$$h = p_z - d_1 \quad (13)$$

Where:  $p_x$ ,  $p_y$ ,  $p_z$  are 3D positions of an object. The limit angle values of the joints are shown in Table 2 [17].

Table 2. Limit angles of the joints

Joint	Minimum Angle (Degree)	Maximum Angle (Degree)
$\theta_{\text{base}}$	0	$\pi$
$\theta_{\text{shoulder}}$	$\pi/9$	$8\pi/9$
$\theta_{\text{elbow}}$	0	$\pi$

#### 2.3.4. Trajectory Planning of the Robotic Arm

The robotic arm executes three movements for each object. A trajectory planning has been performed for each movement. The first movement is from initial position to the position required to pick the object, the second movement is from where the object is picked to where the object is placed, the last movement is from where the object is placed to initial position. The first and last trajectories are planned only on the initial and target positions, while the second trajectory also uses an intermediate point for the shoulder motor, because it is necessary to avoid other objects. The fifth order polynomial shown in Equation 14 is used in these trajectories [17].

$$\theta(t) = a_0 + a_1 \cdot t + a_2 \cdot t^2 + a_3 \cdot t^3 + a_4 \cdot t^4 + a_5 \cdot t^5 \quad (14)$$

The initial positions of all joints are  $\pi/2$  radians, and the trajectories are completed in 2 seconds. The sampling time of the trajectories is 0.026 seconds. In the second trajectory planning, the slope approach is used to determine velocity at the intermediate point used for the shoulder motor. The speed value at the intermediate point is 5

degrees/second ( $\pi/36$  radians/second). Equations 15, 16 and 17 show the first trajectories of each joint, Equations 18, 19 and 20 show the second trajectories, Equations 21, 22 and 23 show the third trajectories [17-19].

$$\theta_{\text{base}(1)}(t) = 90 + (2,9 \cdot \theta_{\text{base}} - 266,6) \cdot t^3 + (266,6 - 2,9 \cdot \theta_{\text{base}}) \cdot t^4 + (0,8 \cdot \theta_{\text{base}} - 71,1) \cdot t^5 \quad (15)$$

$$\theta_{\text{shoulder}(1)}(t) = 90 + (2,9 \cdot \theta_{\text{shoulder}} - 266,6) \cdot t^3 + (266,6 - 2,9 \cdot \theta_{\text{shoulder}}) \cdot t^4 + (0,8 \cdot \theta_{\text{shoulder}} - 71,1) \cdot t^5 \quad (16)$$

$$\theta_{\text{elbow}(1)}(t) = 90 + (2,9 \cdot \theta_{\text{elbow}} - 266,6) \cdot t^3 + (266,6 - 2,9 \cdot \theta_{\text{elbow}}) \cdot t^4 + (0,8 \cdot \theta_{\text{elbow}} - 71,1) \cdot t^5 \quad (17)$$

$$\theta_{\text{base}(2)}(t) = \theta_{\text{base}} - (2,9 \cdot \theta_{\text{base}}) \cdot t^3 + (2,9 \cdot \theta_{\text{base}}) \cdot t^4 - (0,8 \cdot \theta_{\text{base}}) \cdot t^5 \quad (18)$$

$$\theta_{\text{shoulder}(2)}(t) = \theta_{\text{shoulder}} + (2334,8 - 23,7 \cdot \theta_{\text{shoulder}}) \cdot t^3 + (47,4 \cdot \theta_{\text{shoulder}} - 4657,8) \cdot t^4 + (2481 - 25,3 \cdot \theta_{\text{shoulder}}) \cdot t^5 + 100 + 5 \cdot t + 776,3 \cdot t^3 - 1564,4 \cdot t^4 + 837,5 \cdot t^5 \quad (19)$$

$$\theta_{\text{elbow}(2)}(t) = \theta_{\text{elbow}} + (533,3 - 2,9 \cdot \theta_{\text{elbow}}) \cdot t^3 + (2,9 \cdot \theta_{\text{elbow}} - 533,3) \cdot t^4 + (142,2 - 0,8 \cdot \theta_{\text{elbow}}) \cdot t^5 \quad (20)$$

$$\theta_{\text{base}(3)}(t) = (266,6) \cdot t^3 - (266,6) \cdot t^4 + (71,1) \cdot t^5 \quad (21)$$

$$\theta_{\text{shoulder}(3)}(t) = 135 - (133,3) \cdot t^3 + (133,3) \cdot t^4 - (35,5) \cdot t^5 \quad (22)$$

$$\theta_{\text{elbow}(3)}(t) = 180 - (266,6) \cdot t^3 + (266,6) \cdot t^4 - (71,1) \cdot t^5 \quad (23)$$

### 2.3.5. Interface Program

The system is controlled by an interface program which we call Arm Vision. The program shows images of the objects detected by both cameras, colors and numbers of the objects, positions of the objects relative to the stereo camera system and the robotic arm, and graphs of planned and measured trajectories of each joint. These graphs are updated for each object. When the system completes the process, trajectory graphs of the last object being transported are displayed on the interface. The system is operated with the START button. The application phase of the education kit is carried out by using this interface program and running the system simultaneously. Figure 13 shows an example section of the Arm Vision interface program.

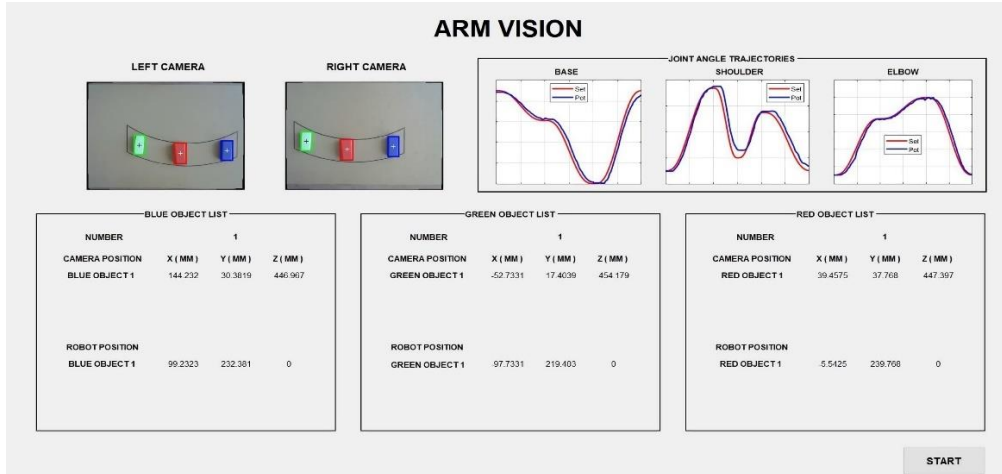


Figure 13. An example section of the Arm Vision interface program

### 3. Experimental Studies and Results

The maximum number of objects that can be placed in the common area is 4. There are three types of objects used in the experimental studies of this paper. These are three rectangular-prism-shaped blue-green-red objects of size 20 mm x 45 mm (width x length), six cube-shaped blue-green-red objects of size 20 mm x 20 mm, one blue cube of size 15 mm x 15 mm (the smallest size that the robotic arm can transport). 10 types of experimental studies were performed which can be listed as follows:

- Same color (blue) - same size objects (45 mm x 20 mm) on the base (1),
- Same color (blue) - same size objects (20 mm x 20 mm) on the base (2),
- Same color (blue) - different size objects on the base (3),
- Different color - same size objects (45 mm x 20 mm) on the base (4),
- Different color - same size objects (20 mm x 20 mm) on the base (5),
- Different color - different size objects on the base (6),
- Same color (blue) - different size objects at 15 mm height (7),
- Different color - different size objects at 15 mm height (8),
- Same color (blue) - different size objects at 45 mm height (9),
- Different color - different size objects at 45 mm height (10).

In each experimental study, 10 experiments were designed and a total of 100 experiments were performed and 91 of them were successfully completed. Table 3 shows experimental results.

Table 3. Experimental results

Experiment	Object Characteristics			Success Rate ( x / 10)
	Number	Color	Size (mm)	
1	2	Blue	45 x 20	10
2	2	Blue	20 x 20	10
3	1	Blue	45 x 20	9
	1	Blue	20 x 20	
	1	Blue	15 x 15	
4	1	Blue	45 x 20	10
	1	Green	45 x 20	
	1	Red	45 x 20	
5	1	Blue	20 x 20	10
	1	Green	20 x 20	
	1	Red	20 x 20	
6	1	Blue	45 x 20	8
	1	Blue	15 x 15	
	1	Green	20 x 20	
	1	Red	20 x 20	
7	1	Blue	45 x 20	10
	1	Blue	20 x 20	
8	1	Blue	45 x 20	8
	1	Blue	15 x 15	
	1	Green	20 x 20	
	1	Red	20 x 20	
9	1	Blue	45 x 20	8
	1	Blue	20 x 20	
	1	Blue	15 x 15	
10	1	Blue	45 x 20	8
	1	Green	20 x 20	
	1	Red	20 x 20	

Fail experiments are due to the end effector. A video of a sample experiment can be found in the reference [20]. Figure 14 (a), (b), (c) and (d) shows the transport steps of

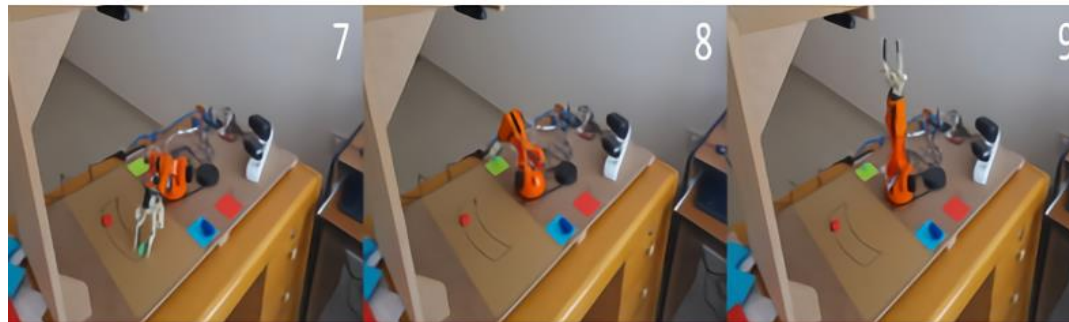
the objects for a sample study with four objects. In order to test the accuracy of the system, several pick-and-place experiments were also performed by holding a 20 mm x 45 mm blue object with a human hand at arbitrary positions. All of these several experiments were successfully completed. Figure 15 shows the transport steps of one of the experiments performed by holding the object with a human hand at arbitrary positions.



(a)



(b)



(c)



(d)

Figure 14. Transport steps of the (a) first, (b) second, (c) third and (d) fourth objects at a sample study with four objects. The system has been set to transport the blue objects firstly, then the green objects, and then the red objects.

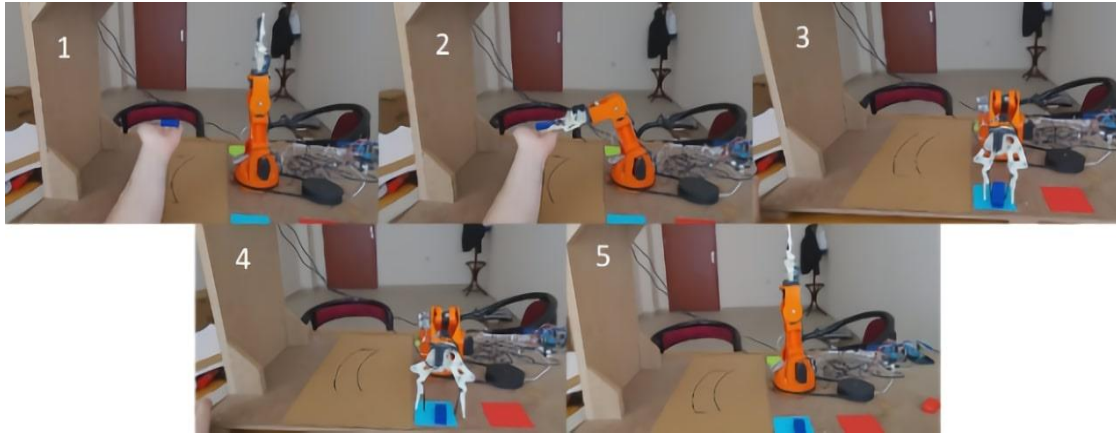


Figure 15. Transport steps of one of the experiments performed by holding the object with a human hand at arbitrary positions.

#### 4. Conclusions

In this paper, a robotic-based education kit with eye-to-hand configuration has been developed. In this kit, colors and positions of the objects of various sizes are detected by a stereo camera system, and these objects are classified according to their color by a robotic arm. Within the scope of preparatory studies, motion of the robotic arm was simulated, stereo camera system was calibrated and the workspace was determined. Also, measurement test of the potentiometers was performed and the error rates in the base, shoulder and elbow joints were 3%, 0.6% and 0.5% respectively. Within the scope of experimental studies, 100 experiments were performed with this stereo-camera-enhanced pick-and-place system and 91 of which were successfully completed. Fail experiments are entirely due to the structure of the end effector. This



problem can be solved by replacing the plastic part of the end effector with other plastics or using another end effector. In addition, several experiments were performed by holding an object with a human hand at arbitrary positions. The camera system precisely detected the 3D position of this object, and the robotic arm picked it and placed on the target point. The system is suitable for educations in the fields of engineering such as object recognition, forward - inverse kinematics, and trajectory planning.

In future studies, the system can be embedded independently of computers. Data display can be improved. Interactive systems with people can be created by establishing collaborative robotic systems. Number of stereo camera systems can be increased to provide the ability to see the entire area by a robotic arm. A stereo camera system can be mounted on the end effector of a robotic arm instead of being mounted in a fixed position to give the robotic arm the ability to see all the points it moves around.

### **Acknowledgment**

This paper was supported by Karabuk University Scientific Research Projects Coordinator within the scope of KBU BAP-18-YL-054. The authors would also like to thank Prof. Dr. Raif BAYIR for his fruitful advices.

### **References**

- [1] Yavuz E. Control of 3-dof (3R) robot manipulator and moving objects based on image processing, MS. thesis, Dokuz Eylül University, Graduate School of Natural and Applied Science, 2015.
- [2] Global collaborative robots market 2017-2021, Technavio Report, London, 2017.
- [3] Global industrial robot sensors market 2017-2021, Technavio Report, London, 2017.
- [4] Şenel FA, Cetisli B. Object control on production line with image processing and five axis robot arm, Pamukkale University Journal of Engineering Sciences 2015; 21: 158-161.
- [5] Lin, C.C., Gonzalez, P., Cheng, M.Y., Luo G.Y., Kao, T.Y., 2016, Vision based object grasping of industrial manipulator, *2016 International Conference on Advanced Robotics and Intelligent Systems (ARIS)*, Taipei-Taiwan, 1-5.
- [6] Taryudi, Wang, M.S., 2017, 3D object pose estimation using stereo vision for

object manipulation system, *2017 International Conference on Applied System Innovation (ICASI)*, Sapporo-Japan, 1532-1535.

[7] Shi G., Chen D., 2017, Research and applications of the hybrid cameras visual servo robot, *2017 8th International Conference on Mechanical and Intelligent Manufacturing Technologies (ICMIMT)*, Cape Town-South Africa, 74-79.

[8] Chang WC, Cheng MY, Tsai HJ. Image feature command generation of contour following tasks for SCARA robots employing image-based visual servoing - a PH-spline approach, *Robotics and Computer-Integrated Manufacturing* 2017; 44: 57-66.

[9] Ali HM, Aizat K, Yerkhan K, Zhandos T, Anuar O. Vision-based robot manipulator for industrial applications, *Procedia Computer Science* 2018; 133: 205-212.

[10] Luo G.Y., Cheng M.Y., Chiang C.L., 2017, Vision-based 3D object pick-and-place tasks of industrial manipulator, *2017 International Automatic Control Conference (CACs)*, Pingtung-Taiwan, 1-7.

[11] Fei Z., Zhou X., Gao X., Zhang G., 2017, A flexible 3D laser scanning system using a robotic arm, *SPIE 10329, Optical Measurement Systems for Industrial Inspection X, 103294U*.

[12] Kang S., Kim K., Lee J., Kim J., 2016, Robotic vision system for random bin picking with dual-arm robots, *2016 International Conference on Measurement Instrumentation and Electronics (ICMIE 2016)*, Munich-Germany, 1-5.

[13] Dinham M., Fang G., 2015, Simultaneous calibration of a stereo vision system and a welding robot-an automated approach, *International Conference on Robotic Welding, Intelligence and Automation*, Shanghai-China, 197-211.

[14] 2020 MATLAB Documentation website. [Online], <https://www.mathworks.com/help/matlab>

[15] Alagoz BB. A note on depth estimation from stereo imaging systems, *Journal of Computer Science* 2016; 1: 8-13.

[16] 2020 MATLAB Computer Vision Toolbox website. [Online], <https://www.mathworks.com/help/vision/index.html>

[17] Bingul Z, Kucuk B. *Robot Kinematics*. Istanbul: Birsen Publisher; 2009.

[18] Yavuz S. A transformation matrices module in position analysis of serial manipulators for denavit-hartenberg method, *In Progress* 2016.

[19] Uzuner S, Akkuş N, Toz M. Trajectory planning of a 5-DOF serial robot

manipulator in joint-space, *Journal of Polytechnic* 2017; 20: 151-157.

[20] The video of one sample experiment performed by the developed system can be found at: [https://yadi.sk/i/\\$Xk9XM3kmuuvow](https://yadi.sk/i/$Xk9XM3kmuuvow)

[21] 2020 Robotics Toolbox for MATLAB website. [Online], <https://petercorke.com/toolboxes/robotics-toolbox>